J. Fluid Mech. (1986), *vol.* 169, *pp.* 379–407
Printed in Great Britain

Rotating flows along indented coastlines

By JOSEF CHERNIAWSKY† AND PAUL H. LEBLOND
Department of Oceanography, University of British Columbia, 6270 University Boulevard, Vancouver, B.C., Canada V6T 1W5

(Received 20 February 1985 and in revised form 4 February 1986)

We examine the problem of a steady, inviscid, reduced-gravity rotating flow in a wedge around a sharp corner. Solutions to nonlinear equations are obtained via a power-series expansion in a Rossby number, diffraction theory and Green's function method. The wedge of an angle $\frac{3}{2}\pi$ is used, as an example, to show details of the solution. The results exhibit the relative importance of the pressure gradient, centrifugal and Coriolis forces. For re-entrant corners, a centrifugal upwelling of the interface occurs very close to the apex and, hence, is not important if coastal radii of curvature are comparable to, or larger than, the Rossby radius; the flow is also supercritical within an arc, whose size depends upon the Rossby number and the angle of the wedge. Using two or more corner solutions, plausible flow streamlines can be generated in more complicated domains, as long as no two corners are closer than the Rossby radius of deformation. This procedure is illustrated with two examples: (i) circulation in a channel mouth; and (ii) flow around a square bump in a coastline.

1. Introduction

Large-scale models of ocean circulation necessarily ignore many details of coastal geometry. Although the main features of oceanic gyres are almost certainly independent of the precise geometry of coastlines, the boundary currents which form part of these gyres may be deflected or bifurcated by promontories or submerged features. The channelling of a significant part of the western boundary current of the North Atlantic mid-latitude gyre by the Strait of Florida and the influences of the Charleston bump (Janowitz & Pietrafesa 1982) on the Gulf Stream provide familiar illustrations of the above statement. Further striking examples of how boundary currents follow a coastline and loop into wide sea straits are provided by the western part of the sub-polar gyre of the North Atlantic (figure 1). The East Greenland Current hugs the coast of Greenland to transform itself into the West Greenland Current, which continues into and around Baffin Bay to flow outwards as the Baffin and then the Labrador Current. Along its course the Baffin Current loops in and out of Lancaster Sound at its northern end (Fissel, Lemon & Birch 1982) and Hudson Strait further south (LeBlond 1980; LeBlond *et al.* 1981). It is the nature of these deflections by headlands and into channels which is the subject of this paper. We examine the behaviour of model flows around single wedges of arbitrary angles and near pairs of wedges which simulate the entrance to side channels such as Hudson Strait and Lancaster Sound. The re-entrant circulation observed in these channels has been documented by iceberg drift observations (Marko, Birch & Wilson 1982),

† Present address: G.A.Borstad Associates, 10474 Resthaven Drive, Sidney, B.C., Canada V8L 3H7.

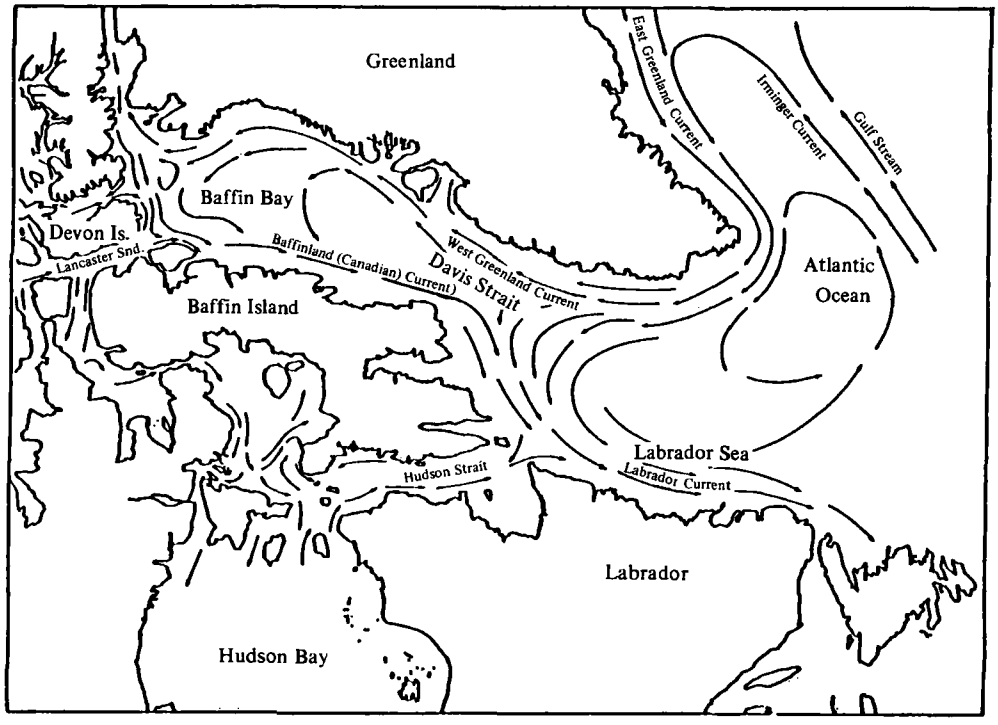

FIGURE 1. The western part of the sub-polar gyre of the North Atlantic.

the distribution of water properties (Osborn *et al.* 1978; Fissel *et al.* 1982), and flow measurements from drifting and moored instruments (LeBlond *et al.* 1981; Fissel *et al.* 1982; Drinkwater 1985). The analysis of their mean flow characteristics is a first step in understanding the complex dynamics of these areas.

The formulation is similar to that used by Whitehead, Leetmaa & Knox (1974), Gill (1977), Nof (1978*a*, *b*) and Roed (1980) to study the rotational hydraulics of channel flows, but is not restricted to slowly varying coastlines: the full two-dimensional problem is treated here. Whitehead *et al.* (1974) derived depth and velocity profiles inside a channel as functions of the upstream depth. Nof solved two-dimensional problems of a steady one-layer outflow over a step (1978*a*) and of a two-layer outflow (1978*b*) from a channel into a wider basin, with velocity profiles prescribed in the mouth of the channel. Gill (1977) derived solutions for the case of a hydraulic control by a weir in a channel with slowly varying width and depth. Roed (1980) did a similar analysis for the case of a single coastline with a slowly varying curvature and depth profile. Nof & Olson (1983) used conservation of integrated momentum to calculate transports through broad passages between oceans and marginal seas, although they did not attempt to describe details of the flow in the passage itself. We are aware of only one example of a detailed analytical solution for the flow around a fast-changing coastline. Hughes (1981, 1982) has modelled an upper layer flow with separation (and a downstream control by another coastline) around a sharp corner on a low-latitude f-plane; i.e. in the limit of slow rotation. We endeavour to do the same here, but for the case of a mid- to high-latitude f-plane, where the stronger Coriolis force tends to keep the boundary current attached to the coast on its right, even around corners with significant curvatures. In the next section, we derive

equations of motion for the case of a non-uniform potential-vorticity coastal flow with an exponential profile, which decays offshore with a scale given by a modified Rossby radius. The resulting nonlinear equations are then expanded in a power series in ϵ, a Rossby number based on this scale. The solution for a flow around an arbitrary corner is derived in §3, using diffraction and Green's function methods. In §4 we show how to combine these solutions to model flows in channel mouths and around irregular coastlines.

2. The governing equations

Our analysis of coastal flows is based on the conservation principles that govern the steady inviscid motion of an incompressible fluid in a rotating frame of reference. These are Bernoulli's equation

$$\tfrac{1}{2}(u^2+v^2)+g'h = G(\psi), \tag{2.1}$$

and the potential vorticity equation

$$\frac{v_x-u_y+f}{h} = K(\psi). \tag{2.2}$$

Their derivation can be found in standard textbooks (e.g. Pedlosky, 1979, p. 64; Gutman 1972). Here u and v are the horizontal velocity components, h is the thickness of the moving layer, f the Coriolis parameter, $g' = (\Delta\rho/\rho)g$ the reduced gravity, and ψ the transport stream function whose definition through

$$hv = \psi_x, \quad -hu = \psi_y \tag{2.3}$$

is a direct consequence of the volume conservation principle

$$(hu)_x+(hu)_y = 0. \tag{2.4}$$

$G(\psi)$ and $K(\psi)$ are functions of integration that are derived from the upstream conditions. They are not independent but are connected through $K(\psi) = G'(\psi)$ (Charney 1955; Gutman 1972). This last relation can be derived by differentiating (2.1) with respect to x and then combining the result with the x momentum equation,

$$uu_x+vu_y-fv = -g'h_x,$$

while using (2.3) and the chain rule, $G_x = G_\psi \psi_x$. Finally, the boundary condition at the coast is specified by assuming it to be a streamline.

2.1. *The upstream profile*

LeBlond (1980) showed that when a coastal current is in a geostrophic balance with the pressure gradient due to a linearly sloping interface (figure 2*a*), then the interface meets the surface at a distance X, given by

$$X = \frac{R}{F} = \frac{C^2}{fV}, \tag{2.5}$$

where $R = C/f$ is the Rossby deformation radius, $F = V/C$ is the Froude number based on the velocity $C = (g'H)^{\frac{1}{2}}$ of long internal gravity waves, and V and H are, respectively, the flow speed and thickness at the coastal boundary. In order to allow for a smooth transition between the coastal current and the offshore region, we assume

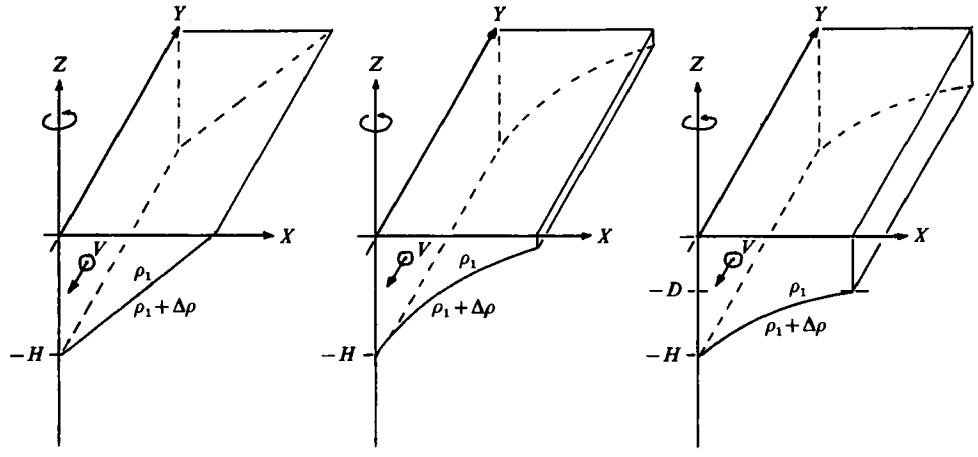

FIGURE 2. Three profiles of the upper-layer depth: (*a*) linear $h = H(1-x/X)$, (*b*) exponential $h = He^{-x/X}$ and (*c*) exponential $h = D+He^{-x/X}$.

that the interface depth decreases exponentially offshore (figure 2*b*) with the same scale X,

$$h(x) = He^{-x/X}. \tag{2.6}$$

Assuming geostrophy, we also get

$$v(x) = \frac{g'h_x}{f} = -Ve^{-x/X}, \tag{2.7}$$

where $V = g'H/fX = FC$ if we use (2.5). When the first equation in (2.3) is integrated with respect to x, we find that the transport stream function is given by

$$\psi(x) = Qe^{-2x/X}, \tag{2.8}$$

with the arbitrary constant set to zero. Note that $Q = \psi(0) = \frac{1}{2}VHX$ is also the total transport in a triangular profile (figure 2*a*), which lends support to using X as the horizontal lengthscale. It is worthwhile to note that for an exponential depth profile X remains invariant (i.e. it does not change with the distance offshore) if we replace C and F with their local values

$$c(x) = [g'h(x)]^{\frac{1}{2}} \quad \text{and} \quad F(x) = |v(x)|/c(x).$$

In order to see the connection between the decay scale X and the Rossby radius of deformation, used by many authors as a lateral scale for coastal flows (e.g. Nof 1978*a*, *b*, 1984; Stommel & Luyten 1984), we consider (for a moment) a current thickness that is given by

$$h(x) = D+He^{-x/X}, \tag{2.9}$$

where D is some non-zero constant reference depth (figure 2*c*). If we now assume a uniform potential vorticity, then, for the one-dimensional case, (2.2) becomes

$$\frac{v_x+f}{h} = \frac{f}{D}. \tag{2.10}$$

But $v_x = (V/X)e^{-x/X}$ and $V/X = F^2f$, so that from (2.10) we get

$$\frac{f}{D}(1+F^2e^{-x/X})/\left(1+\frac{He^{-x/X}}{D}\right) = \frac{f}{D}, \tag{2.11}$$

or
$$\frac{H}{D} = F^2. \tag{2.12}$$

Hence,
$$X = \frac{R}{F} = \frac{(g'D)^{\frac{1}{2}}}{f}, \tag{2.13}$$

i.e. in this case, X *is* the Rossby radius based on the reference depth D. We note that for $F < 1$, $H < D$, so that for a vanishing D (figure 2*b*) the uniform potential vorticity equation (2.10) is not applicable, R_D is meaningless and X as defined by (2.5) is the natural decay scale. By defining a potential depth $H_p = H/F^2$, we get $X = (g'H_p)^{\frac{1}{2}}/f$, so that in a wider sense we can call X a Rossby deformation radius (based on H_p). The use of the 'potential depth' in constant-potential-vorticity models, though not always so named, is not new (e.g. Stommel 1965; Flierl 1979; Gill & Schumann 1979; Stommel & Luyten 1984).

We now use (2.6)–(2.8) in the one-dimensional versions of (2.1) and (2.2) and obtain

$$G(\psi) = (g'f)^{\frac{1}{2}}(2\psi)^{\frac{1}{2}} + F^2\left(\frac{f}{H}\right)\psi, \tag{2.14}$$

and
$$K(\psi) = (g'f)^{\frac{1}{2}}(2\psi)^{-\frac{1}{2}} + F^2\left(\frac{f}{H}\right). \tag{2.15}$$

When these are combined with (2.1) and (2.2) we get a pair of nonlinear equations which together with (2.3) and some prescribed boundary conditions (to be specified later) define the physical problem of inviscid rotational flow along a coast.

2.2. *Scaling and derivation of the governing equations*

We non-dimensionalize the variables according to

$$(x, y) = X(x', y'), \quad (u, v) = V(u', v'), \quad h = Hh', \quad \psi = Q\psi'. \tag{2.16}$$

Substitution into (2.1)–(2.3) gives (after dropping the primes) the non-dimensional equations

$$h + \tfrac{1}{2}\epsilon(u^2 + v^2) = \psi^{\frac{1}{2}} + \tfrac{1}{2}\epsilon\psi, \tag{2.17}$$

$$1 + \epsilon(v_x - u_y) = h\psi^{-\frac{1}{2}} + \epsilon h, \tag{2.18}$$

$$2vh = \psi_x, \quad -2uh = \psi_y. \tag{2.19}$$

We have used $\epsilon = F^2 = V/fX$, a Rossby number that is based on X. We eliminate square roots by changing to a new stream-function variable s according to

$$\psi = s^2. \tag{2.20}$$

As a result, (2.17)–(2.19) become

$$2h + \epsilon(u^2 + v^2) = s(2 + \epsilon s) \tag{2.21}$$

$$s[1 + \epsilon(v_x - u_y)] = h(1 + \epsilon s) \tag{2.22}$$

$$vh = ss_x, \quad -uh = ss_y. \tag{2.23}$$

We consider s, h, u and v as regular functions of the Rossby number ϵ, expressing them in a regular perturbation expansion of the form

$$(s, h, u, v) = \sum_{i=0}^{\infty} \epsilon^i (s_i, h_i, u_i, v_i). \tag{2.24}$$

As a result, we get from (2.21) to orders ϵ^0, ϵ^1 and ϵ^2, respectively

$$h_0 = s_0, \tag{2.25a}$$

$$2h_1 + u_0^2 + v_0^2 = 2s_1 + s_0^2, \tag{2.25b}$$

$$h_2 + u_0 u_1 + v_0 v_1 = s_2 + s_0 s_1. \tag{2.25c}$$

From (2.22), we obtain

$$s_0 = h_0, \tag{2.26a}$$

$$s_1 + s_0(v_{0x} - u_{0y}) = h_1 + h_0 s_0, \tag{2.26b}$$

$$s_2 + s_1(v_{0x} - u_{0y}) + s_0(v_{1x} - u_{1y}) = h_2 + h_1 s_0 + h_0 s_1. \tag{2.26c}$$

Finally, the continuity equations (2.23) yield

$$v_0 h_0 = s_0 s_{0x}, \quad -u_0 h_0 = s_0 s_{0y}, \tag{2.27a}$$

$$v_0 h_1 + v_1 h_0 = (s_0 s_1)_x, \quad -u_0 h_1 - u_1 h_0 = (s_0 s_1)_y. \tag{2.27b}$$

We can now use these equations to get a single equation for the $O(1)$ stream-function variable s_0 and another one for the $O(\epsilon)$ contribution s_1. From either (2.25a) or (2.26a), we get

$$h_0 = s_0, \tag{2.28}$$

which shows that the $O(1)$ interface depth is a streamline. As a result, from (2.27a) we obtain the $O(1)$ velocities,

$$v_0 = s_{0x}, \quad -u_0 = s_{0y}, \tag{2.29}$$

so that, at least to this order, the flow is geostrophic. Consequently, we also get the $O(1)$ relative vorticity

$$v_{0x} - u_{0y} = \nabla^2 s_0 \tag{2.30}$$

and the $O(1)$ kinetic energy

$$U_0 = \tfrac{1}{2}(u_0^2 + v_0^2) = \tfrac{1}{2}(\nabla s_0)^2. \tag{2.31}$$

From (2.25b) it follows that the $O(\epsilon)$ layer depth is related to s_1 via

$$h_1 = s_1 + \tfrac{1}{2}[s_0^2 - (\nabla s_0)^2], \tag{2.32}$$

while, from (2.26b), we find

$$h_1 = s_1 + s_0(\nabla^2 s_0 - s_0). \tag{2.33}$$

We combine the last two equations to obtain the differential equation for s_0:

$$\nabla^2 s_0 - s_0 = \frac{s_0^2 - (\nabla s_0)^2}{2s_0}. \tag{2.34}$$

Even to this leading order, the equation is nonlinear. This nonlinearity can be traced back to the non-uniformity of the potential vorticity, which is a consequence of (2.6). From (2.32) we see that the right-hand side of (2.34), which looks like the departure of the $O(1)$ kinetic energy from its value upstream (divided by the depth h_0, see (2.17) and (2.25b)), is also the $O(\epsilon)$ departure of the depth h from the streamline s, and this difference contributes to the balance between the relative vorticity term, $\nabla^2 s_0$, and the vortex stretching term s_0 ($= h_0$). As we shall see in the next section, the right-hand side of (2.34) vanishes whenever the motion is rectilinear, which is the case upstream or far from boundaries. In particular, upstream, where $h = s$ identically, $h_1 = s_1 = 0$ and hence the relative vorticity is equal to s and the kinetic energy is equal

to $\frac{1}{2}s^2$. Following the same method, it is not difficult to show that in the case of a uniform potential-vorticity function $K(\psi)$, the right-hand side of (2.34) vanishes and hence the $O(1)$ equation for s_0 is linear.

The derivation of the equation for s_1 is given in the Appendix. The result is

$$s_0 \nabla^2 s_1 + \nabla s_0 \cdot \nabla s_1 + (\nabla^2 s_0 - 3s_0)\, s_1 = W, \tag{2.35}$$

where (see the Appendix)

$$W = \frac{[s_0^2 - (\nabla s_0)^2]^2}{4s_0} + s_0^3 - \tfrac{1}{2}(\nabla s_0 \cdot \nabla)\,(\nabla s_0)^2. \tag{2.36}$$

The function W can be rewritten more concisely as

$$W = s_0(M^2 + s_0^2) - (\nabla s_0 \cdot \nabla)\, U_0, \tag{2.37}$$

where $M = \frac{1}{2}s_0 - U_0/s_0$ is the right side of (2.34) and U_0 is the $O(1)$ kinetic energy, given by (2.31). It can be shown that when the flow is rectilinear, W vanishes identically, together with M.

We can linearize (2.34) and simplify the left side of (2.35) if we use transformations

$$s_0 = p^{\frac{2}{3}} \tag{2.38}$$

and

$$s_1 = p^{-\frac{1}{3}} q. \tag{2.39}$$

These result in two modified Helmholtz equations, an homogeneous one for the $O(1)$ stream-function variable p,

$$\nabla^2 p - (\tfrac{3}{2})^2 p = 0, \tag{2.40}$$

and an inhomogeneous one for the $O(\epsilon)\, q$,

$$\nabla^2 q - (\tfrac{3}{2})^2 q = p^{-\frac{1}{3}} W. \tag{2.41}$$

Also, since $s^2 = \psi = \psi_0 + \epsilon\psi_1 + \ldots$, we get

$$\psi_0 = p^{\frac{4}{3}}, \quad \psi_1 = 2p^{\frac{1}{3}} q. \tag{2.42}$$

Equations (2.38)–(2.42) define the physical problem if the shape of the domain and the boundary conditions are specified.

3. Rotating flow around a sharp bend

We proceed now to solve the problem, stated in the previous section, for the particular case of a domain bounded by two straight walls, which are located at $\theta = 0$ and $\theta = \pi/a$, with $a > \frac{1}{2}$. As stated previously, we assume that a geostrophic current with an exponential depth profile, given by (2.6), approaches the bend from upstream, with the $\theta = \pi/a$ boundary on its right. We also assume that, unless it should appear explicitly from the solution of the problem, there is no separation of streamlines from the bounding wall. Consequently, the current turns the bend, even for a re-entrant corner, and the far-downstream depth profile is identical with that far upstream of the corner.

The equations to be solved are (2.40) and (2.41). The boundary condition at the wall is $s = 1$, which can be expanded to give

$$p = 1 \quad \text{at } \theta = 0, \pi/a \tag{3.1}$$

and

$$q = 0 \quad \text{at } \theta = 0, \pi/a. \tag{3.2}$$

3.1. *The O(1) solution*

Before we start, it should be pointed out that (2.40) and (3.1) are connected with the problem of diffraction of a Kelvin wave by a wedge. The latter was solved by Roseau (1967) and also by Packham & Williams (1968) for a general wedge angle using a complex integral representation. Buchwald (1968) used the Wiener–Hopf technique to solve the diffraction problem for the particular case of a Kelvin wave incident at a right-angled corner. In principle, the solution of our problem should be obtainable from the latter by a limiting process, wherein the Kelvin wave transforms into a geostrophic current with an exponential profile, in the limit of zero frequency. Unfortunately, owing to its complexity, only asymptotic forms of the wave solution were presented in the above papers.

The methods employed by Roseau and by Packham & Williams are related to the 'Sommerfeld diffraction problem', which deals with the diffraction of electromagnetic waves by a conducting wedge. Sommerfield (1896) solved it for the case of a half-screen (wedge of an angle 2π) and also showed how to do it for an angle which is a submultiple of $2n\pi$, where n is a positive integer (for an illuminating discussion, the reader is referred to Sommerfeld 1954, §38). His method was generalized to an arbitrary angle by Macdonald (1915), Bromwich (1915), Whipple (1916) and Carslaw (1919). Some of the extensive literature on the subject was reviewed by Oberhettinger (1954).

Since we chose to use the results of diffraction theory, we briefly review its formulation. We need consider only the special case of a plane wave of unit strength, $F_0 = \exp\{ik[ct + r\cos(\theta - \theta_0)]\}$, incident from the direction θ_0 at a right angle to an edge of the wedge. After removal of the time dependence, the Sommerfeld diffraction problem reduces to solving the Helmholtz equation,

$$\nabla^2 P + k^2 P = 0, \tag{3.3}$$

subject to the condition that the solution P is zero on each boundary.

Bromwich (1915) used the case of the wedge π/n, where n is a positive integer, as a starting point of the familiar method of images. He replaced the sum of the images by a complex integral and then extended his formulae to hold for any (real and positive) value of $n = a$. Subsequently, by deforming the integration path, Whipple (1916) was able to show that the solution can be written as

$$\begin{aligned} P = {} & \text{'sum of visible images'} \\ & - F(\pi + \theta - \theta_0) - F(\pi - \theta + \theta_0) + F(\pi - \theta - \theta_0) + F(\pi + \theta + \theta_0), \end{aligned} \tag{3.4}$$

where the diffraction terms F are given by

$$F(\phi) = \frac{a \sin(a\phi)}{2\pi} \int_0^\infty \frac{\exp(-ikr\cosh u)\,du}{\cosh(au) - \cos(a\phi)}, \tag{3.5}$$

and the 'visible images' are the incident wave F_0 and its images that are 'visible' at (r, θ). Whipple also showed that each diffracted term $F(\phi)$ satisfies (3.3).

In order to solve the boundary-value problem, defined by (2.40) and (3.1), we change k to ik, ($k = \frac{3}{2}$ in (2.37)) and describe the incoming current as an evanescent plane 'wave' emanating from the boundary at $\theta = \pi/a$. Thus the 'wave source' is presumed to 'radiate' from the direction $\theta_0 = \pi/a + \frac{1}{2}\pi$ (figure 3), in which case

$$F_0 = \exp[kr\cos(\theta - \theta_0)] = \exp\left[kr\sin\left(\theta - \frac{\pi}{a}\right)\right]. \tag{3.6}$$

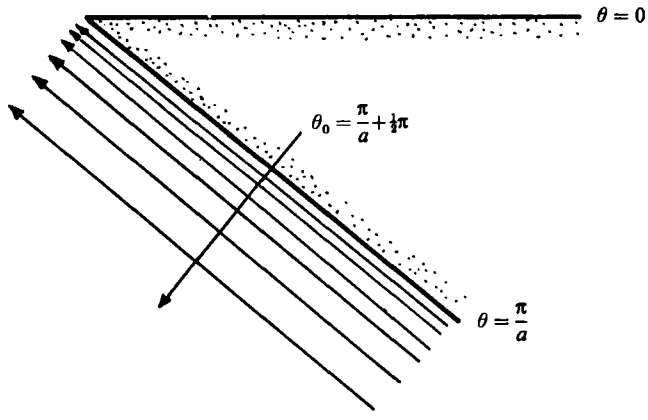

FIGURE 3. The incoming current profile as an evanescent 'wave' emanating from the boundary along $\theta = \pi/a$.

As a result, the diffracted term (3.5) becomes (see Whipple 1916 for details)

$$F(\phi) = \frac{a \sin(a\phi)}{2\pi} \int_0^\infty \frac{\exp(ikr \sinh u)\, du}{\cosh(au) - \cos(a\phi)}. \tag{3.7}$$

Owing to the difference in boundary conditions ($p = 1$, while $P = 0$ on $\theta = 0, \pi/a$), we cannot use (3.4) directly, but must seek an alternate combination of F-terms. We investigate first the functional behaviour of $F(\phi)$, which may be summarized as follows (figures 4*a*, *b*):

(i) $F(\phi)$ is continuous for $0 < \phi < 2\pi/a$ and periodic with a period $2\pi/a$,
(ii) $F(\phi) \to 0$ as $\phi \to \pi/a$, and
(iii) $F(\phi) \to \frac{1}{2}$ as $\phi \to +0$ and $F(\phi) \to -\frac{1}{2}$ as $\phi \to -0$.

Properties (i) and (ii) are readily seen by inspecting (3.7). Property (iii) means that F has a jump discontinuity at $\phi = 0$. This is because as $\phi \to 0$, $\sin(a\phi)$ multiplied by the integral has a finite limit there, while the sin changes its sign. Indeed, if we put $b = \sin(\frac{1}{2}a\phi)$, then, as $b \to 0$, most of the contribution to the integral comes from the vicinity of $u = 0$, in which case $\sinh u \approx u$, $\sinh(\frac{1}{2}au) \approx \frac{1}{2}au$. Taking the real part of (3.7) we get near $b = 0$ (noting that $\sin(a\phi) = 2 \sin(\frac{1}{2}a\phi) \cos(\frac{1}{2}a\phi) \approx 2b$ there)

$$F(b) \approx \frac{ab}{2\pi} \int_0^\infty \frac{\cos(kru)\, du}{(\frac{1}{2}au)^2 + b^2}.$$

Changing to $x = \frac{1}{2}au$, $du = 2dx/a$, we get

$$F(b) \approx \frac{b}{\pi} \int_0^\infty \frac{\cos(2krx/a)\, dx}{x^2 + b^2} = \frac{b}{2|b|} \exp\left(-\frac{2kr|b|}{a}\right). \tag{3.8}$$

Hence, for small ϕ

$$2F(\phi) \approx \operatorname{sign}(\phi) \exp(-kr|\phi|) \to \operatorname{sign}(\phi) \quad \text{as } \phi \to 0.$$

From the above properties of $F(\phi)$, it clearly follows that the solution of the

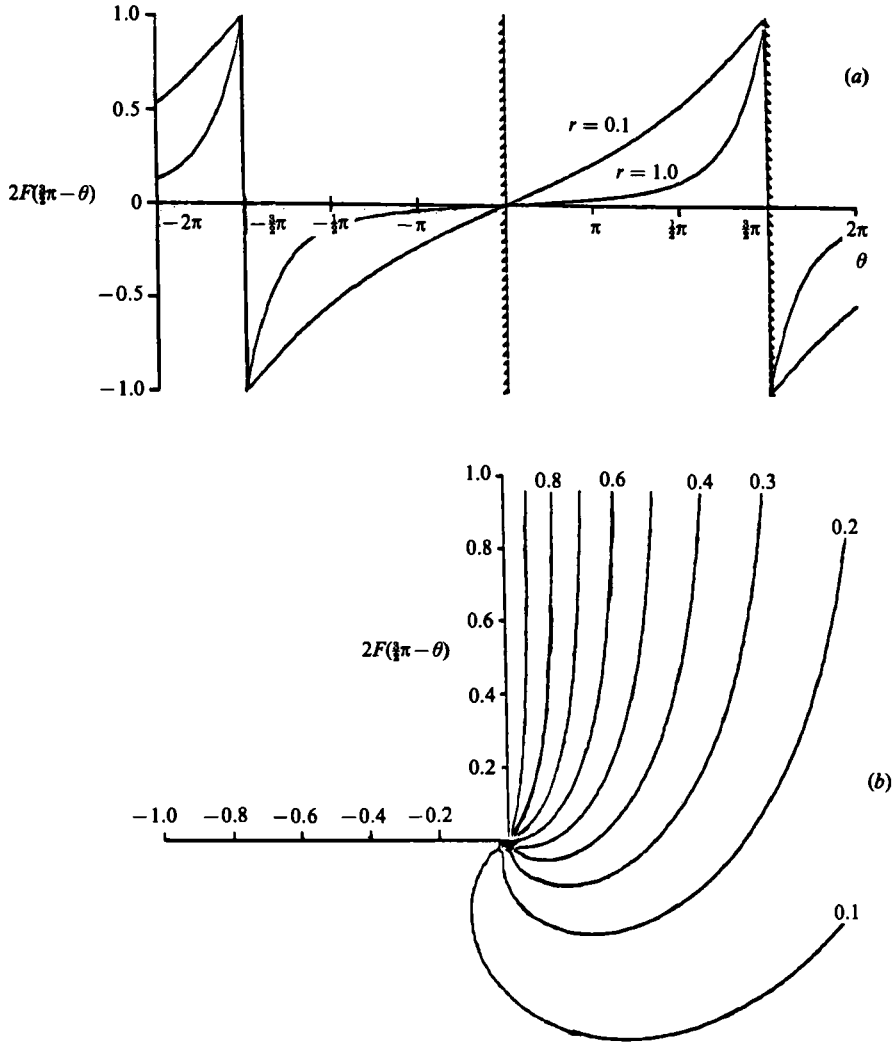

FIGURE 4. Diffraction term $2F(\phi)$, with $\phi = \pi/a - \theta$ and $a = \frac{2}{3}$: (*a*) its functional behaviour in the range $-2\pi < \theta < 2\pi$ for $r = 0.1$ and $r = 1.0$; (*b*) as a rotating sink of a unit strength. The domain is $2X \times 2X$ and contour spacing is 0.1. Unless noted otherwise, the same applies to the subsequent contour plots.

boundary-value problem (2.37) and (3.1) is given by the sum of the four diffraction terms

$$p(r, \theta) = 2F(\theta) + 2F\left(\frac{\pi}{a} - \theta\right),$$

or, explicitly,

$$p = \frac{2\sin(a\theta)}{\pi} \int_0^\infty \frac{\exp[ikr\sinh(u/a)]\cosh u\,\mathrm{d}u}{\sinh^2 u + \sin^2(a\theta)}. \tag{3.9}$$

Since each F-term satisfies (2.37) (with $k = \frac{3}{2}$), then so does p. One can also show this directly by taking derivatives of p with respect to r and θ and substituting back into (2.40). While doing such an exercise, it is useful to know that the value of the integral in (3.9) does not change when its upper limit is replaced by $\infty + id$, with the only condition that $0 < d < a\pi$. This is needed since, when differentiated with respect

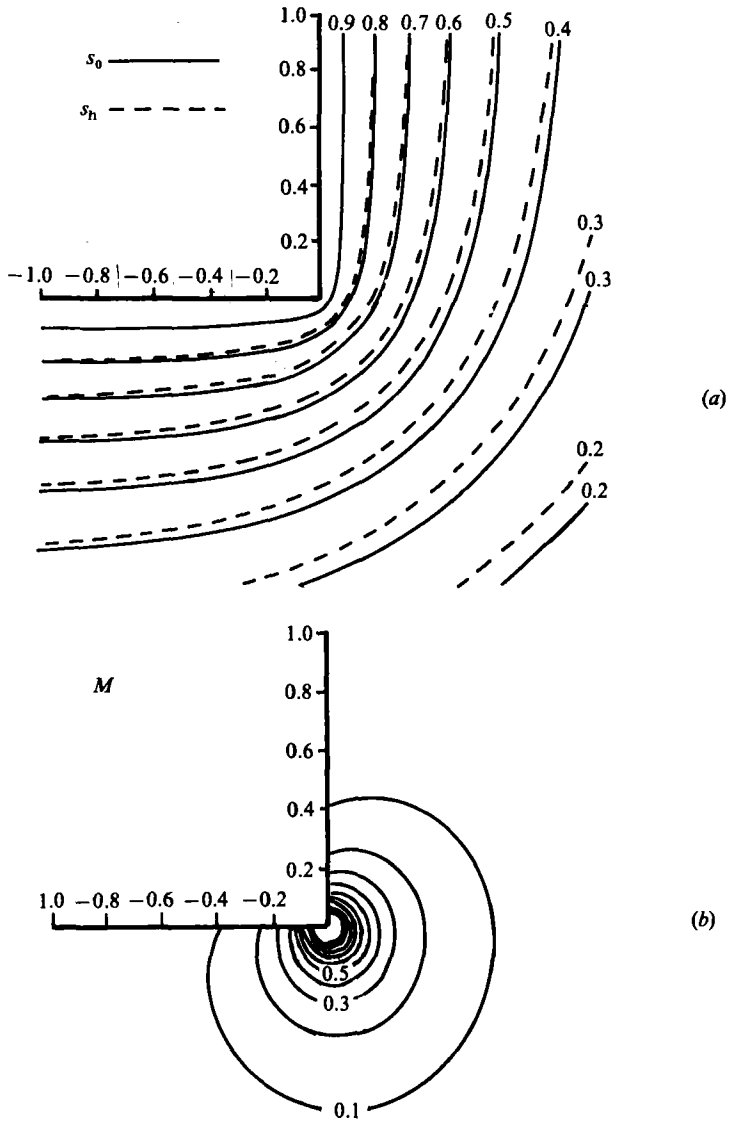

FIGURE 5. (*a*) The $O(1)$ stream function $s_0 = p^{\frac{1}{3}}$ (continuous contours) and its homogeneous counterpart s_h (dashed contours); s_h is the solution of $\nabla^2 s_h - s_h = 0$. (*b*) Contours of $M = [s_0^2 - (\nabla s_0)^2]/2s_0$.

to r, (3.9) gives an apparently divergent integral, which can be transformed into a convergent one by integration by parts, and the integrated terms vanish when the upper limit has this extra $+id$. This is analogous to artificial viscosity, which is often used as a convenient way to get convergence at infinity (see, for example, Carrier, Krook & Pearson 1966, p. 337).

It should be noted that the solution to the boundary-value problem, (2.40) and (3.1), can be written in a number of ways. The more conventional form is a boundary integral of Green's function that is given in terms of modified Bessel functions of a fractional order (see (3.13) in the next section). Alternatively, one can use the Kantorovich–Lebedev transform, which contains a modified Bessel function of an

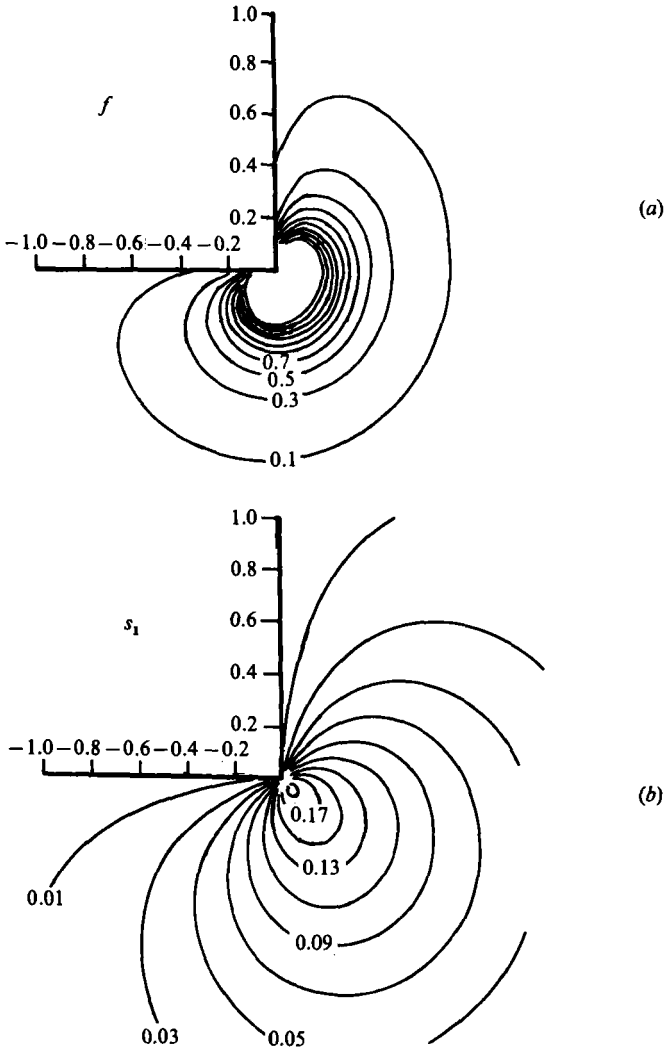

FIGURE 6. (*a*) The right-hand side of (2.38), $f = s_0^{-\frac{1}{2}}W$. (*b*) The $O(\epsilon)$ stream function variable s_1. (*c*) The total transport stream function $\psi = \psi_0 + \epsilon\psi_1$, for $\epsilon = 0.5$. (*d*) Comparison between ψ_0 ($\epsilon = 0$) (broken line) and ψ ($\epsilon = 0.5$) (solid line). [Contour spacings: 0.2 in (*a*) and (*d*), 0.02 in (*b*) and 0.1 in (*c*).]

imaginary order (Stakgold 1968). Therefore, it should be possible to derive (3.9) directly from any of the above. This may be an interesting exercise in itself but is outside the scope of this paper. We only note that (3.9) is easier to compute since it does not involve special functions. Moreover, the diffraction formula of Whipple (1916) may be the shortest way to its derivation.

It is a simple exercise to show that for the particular case of a straight coastline, $a = 1$, (3.9) reduces to the upstream profile $p = \mathrm{e}^{-kx}$, where x is the normal distance to the boundary and $k = \frac{3}{2}$ (hence, $s_0 = \mathrm{e}^{-x}$). For $a \neq 1$, a numerical quadrature can be used to evaluate (3.9) or (3.7). The term $2F(\pi/a - \theta)$ can be thought of as representing a linear rotating flow from the upstream into a sink at the apex of the corner (figure 4*b*). Similarly, $2F(\theta)$ would be a source flow from the apex. Their sum,

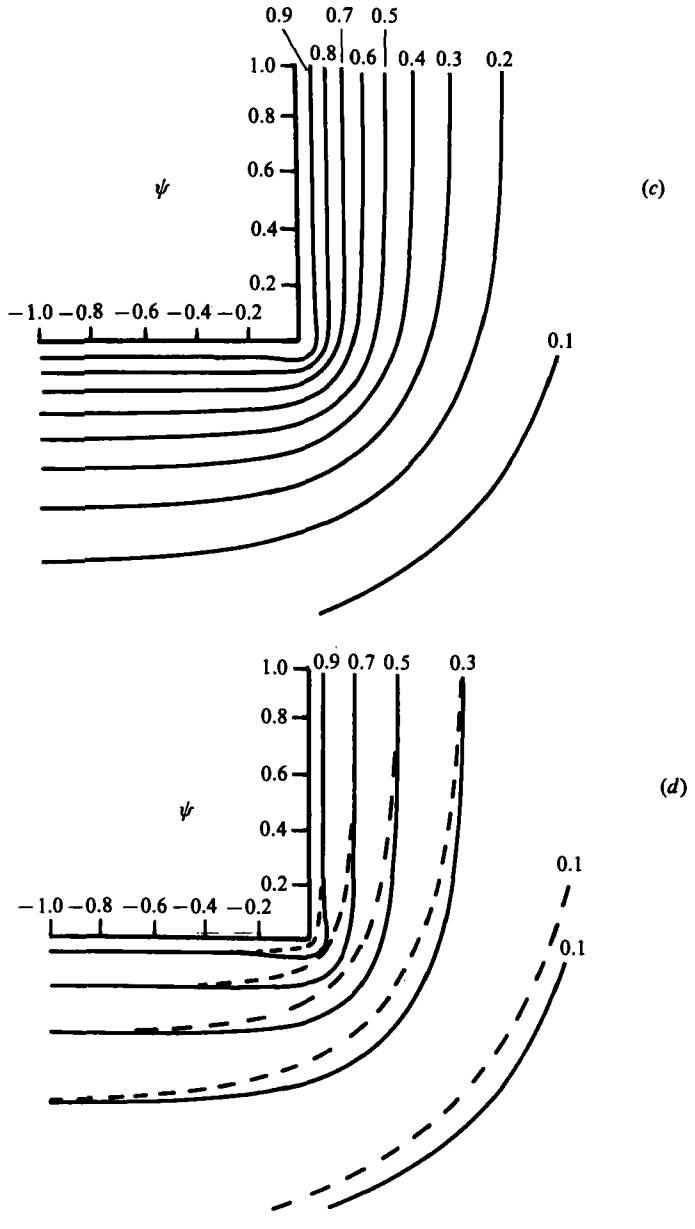

FIGURE 6(*c*) and (*d*). For caption see facing page.

raised to the power $\frac{2}{3}$, according to (2.35), gives s_0, the $O(1)$ stream function, which is plotted on figure 5(*a*) for $a = \frac{2}{3}$ (most of the figures are drawn for this choice of a). s_h, the solution to the homogeneous counterpart of (2.34), is also shown on this figure. The difference between the two is very small, less than 0.03. This means that M, the nonlinear forcing term on the right-hand side of (2.34), plotted on figure 5(*b*), has a small effect on the $O(1)$ solution (it moves the streamlines somewhat away from the corner). As expected, for large r, s_0 reduces to the upstream profile e^{-x}, where x is the distance from either boundary, while for small r it is given by the potential-flow stream function raised to the power $\frac{2}{3}$, $[1-(kr)^a \sin(a\theta)]^{\frac{2}{3}}$.

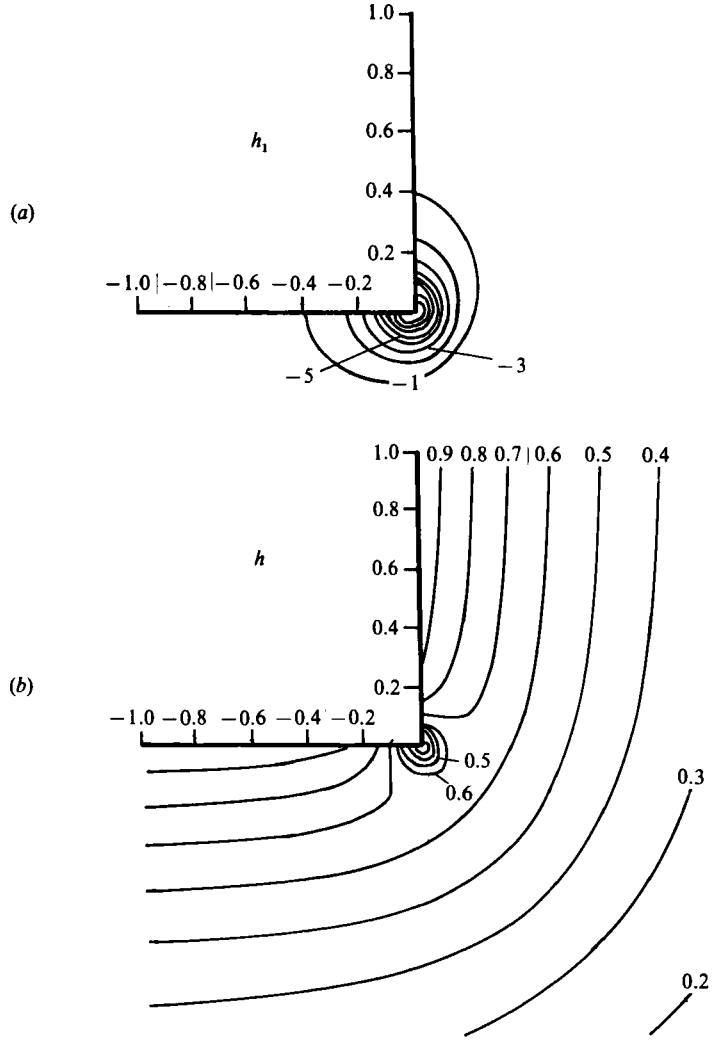

FIGURE 7. (*a*) The $O(\epsilon)$ depth variable h_1; (*b*) contours ($\epsilon = 0.5$); and (*c*) three-dimensional view of the depth of the interface, $h = h_0 + \epsilon h_1$ (*for* $\epsilon = 0.5$).

3.2. *The* $O(\epsilon)$ *solution*

We now proceed to solve the second boundary-value problem, (2.41) and (3.2). Formally, the solution may be written as

$$q(x, y) = \int\int f(x', y')\, G(x, y \,|\, x', y')\, \mathrm{d}x'\, \mathrm{d}y', \tag{3.10}$$

where the integration is over the specified domain, f is the right-hand side of (2.41),

$$f = p^{-\frac{1}{3}} W, \tag{3.11}$$

and W is given by (2.37). The Green's function $G(x, y \,|\, x', y')$ satisfies

$$\nabla^2 G - k^2 G = \delta(x - x')\, \delta(y - y') \tag{3.12}$$

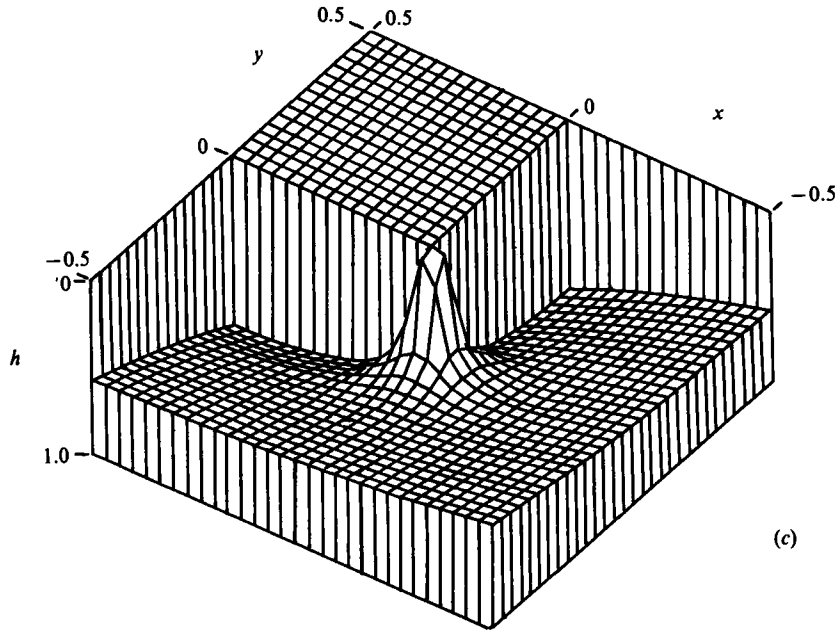

FIGURE 7(*c*). For caption see facing page.

and vanishes on the boundary. It can be written in terms of the modified Bessel functions (see, for example, Stakgold 1968),

$$G(r,\theta\,|\,r',\theta') = -\frac{2a}{\pi}\sum_{m=1}^{\infty}\sin(ma\theta)\sin(ma\theta')\,K_{ma}(kr_>)\,I_{ma}(kr_<), \tag{3.13}$$

with $r_> = \max(r,r')$ and $r_< = \min(r,r')$. Due to the symmetry of the wedge problem, only the odd terms in (3.13) contribute to the integral in (3.10). We will also be satisfied with approximating the $O(\epsilon)$ term q. Calculations show that even if only the leading term in (3.13),

$$G \approx -\frac{2a}{\pi}\sin(a\theta)\sin(a\theta')\,K_a(kr_>)\,I_a(kr_<), \tag{3.14}$$

is retained, the value of q is increased by no more than a few per cent. We compute (3.10) using a simple quadrature routine. Figures 6(*a*,*b*) show contours of the function f and of $s_1 = p^{-\frac{1}{2}}q$ respectively. Somewhat surprisingly, the maximum value of s_1 is less than 0.2, and as a result no separation is evident in the streamlines of $\psi = s_0^2 + 2\epsilon s_0 s_1$, which are shown in figure 6(*c*) for $\epsilon = 0.5$. The only noticeable effect of the $O(\epsilon)$ term on the transport stream function ψ is to move streamlines away from the corner (figure 6*d*), an effect which may be attributed to the centrifugal acceleration of the fluid. Note that since the horizontal scale is $X = R/\epsilon^{\frac{1}{2}}$, statements concerning the $\epsilon = 0$ case should be interpreted in the limiting sense, $\epsilon \to 0$, only.

Using (2.29), we calculate the $O(\epsilon)$ depth,

$$h_1 = s_1 + Ms_0, \tag{3.15}$$

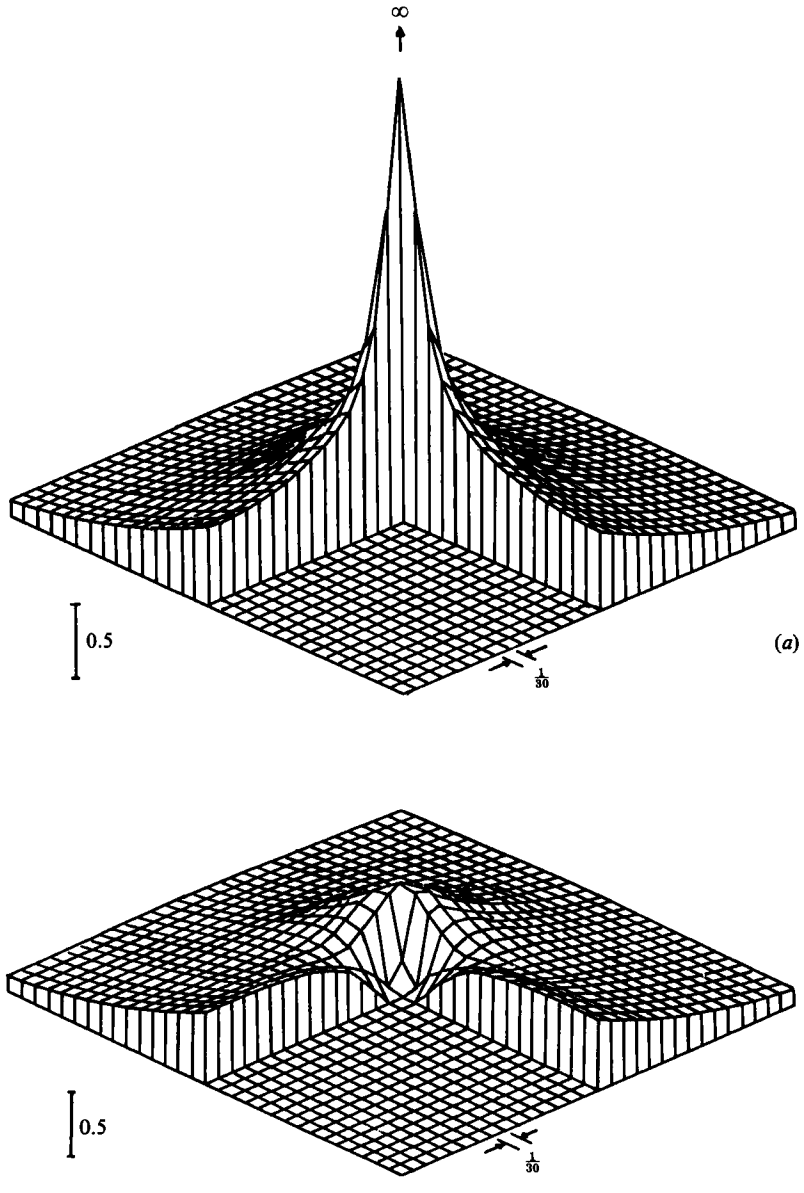

FIGURE 8. Depth-integrated kinetic energy hU: (a) $\epsilon = 0$; (b) $\epsilon = 0.5$. For clarity, the $\frac{1}{2}\pi$ corner was deleted in this figure.

and from (2.27b) and (3.15) we obtain the $O(\epsilon)$ velocities,

$$u_1 = -s_{1y} - Mu_0 \tag{3.15a}$$

and

$$v_1 = s_{1x} - Mv_0. \tag{3.15b}$$

Contours of h_1 are plotted on figure 7 (a), while figures 7 (b, c) show the total depth of the interface $h = h_0 + \epsilon h_1$. The depth-integrated kinetic energy

$$hU = h[(U_0 + \epsilon(u_0 u_1 + v_0 v_1)]$$

is shown on figures 8(*a*, *b*) for the two values of $\epsilon = 0$ and 0.5. Figure 7(*c*) shows clearly the effect of the nonlinear advection terms: a *centrifugal upwelling* for a re-entrant ($a < 1$) corner. In contrast, downwelling would be expected at an inside ($a > 1$) corner. It is also apparent that for large ϵ and/or large corner curvature, we may expect a surfacing of the pycnocline, i.e. separation of the streamlines from the boundary just before or at the corner. This is only vaguely discernible on figure 6(*c*). Owing to the assumed power-series form, (2.21), there is little confidence in the derived solution that close to the corner, where the $O(\epsilon)$ terms are larger than the $O(1)$ terms (see below). This is especially true for re-entrant corners. A separate calculation, which was done for smaller scales (Cherniawsky 1985), shows separation of streamlines very close to the apex. The question of validity of the solution is examined below, while separation is discussed in the end of the section.

3.3. *The validity of the solution*

For a re-entrant corner of infinite curvature, the solution is not valid at the apex, where the velocities u and v are infinite. We must also require that each of the four series in (2.21) converge to a finite limit. We cannot prove convergence of (2.21), but ask instead that the $O(\epsilon)$ terms be of the same order of magnitude, or smaller, than the $O(1)$ terms. Specifically, we require that

$$|s_1| < s_0, \tag{3.16a}$$

$$|h_1| < h_0 = s_0, \tag{3.16b}$$

and

$$|U_1| < U_0, \tag{3.16c}$$

where $U_1 = u_0 u_1 + v_0 v_1$ is the $O(\epsilon)$ kinetic-energy term. Using (3.15*a*, *b*) and (2.29), the last inequality may also be written as

$$|\nabla s_0 \cdot \nabla s_1 - 2MU_0| < U_0. \tag{3.16d}$$

Figures 5(*a*) and 6(*b*) show that (3.16*a*) is satisfied everywhere. Forming the ratios

$$r_1 = \left|\frac{h_1}{h_0}\right| = \left|M + \frac{s_1}{s_0}\right| \tag{3.17}$$

and

$$r_2 = \left|2M - \frac{\nabla s_0 \cdot \nabla s_1}{U_0}\right|, \tag{3.18}$$

we plot contours of r_1 and r_2 on figures 9(*a*, *b*), superimposed upon a few streamlines ψ (for $\epsilon = 0.5$).

These figures show that (depending on ϵ) the solution is valid ($r_1, r_2 < 1$) for relatively (but not infinitely) sharp re-entrant corners, as long as the rounded boundary (e.g. $\psi = 0.9$) streamline does not penetrate inside the curve $r_1 = 1$.

3.4. *Supercritical flow*

Since for a re-entrant corner the velocity of the fluid is high near the apex, we expect the flow to be supercritical there. The local Froude number,

$$Fr = F\left[\frac{u^2 + v^2}{h}\right]^{\frac{1}{2}}, \tag{3.19}$$

is contoured together with ψ on figure 9(*c*). For the chosen flow parameters ($\epsilon = F^2 = 0.5$, $a = \frac{2}{3}$) half of the total transport is passing through the supercritical region, where $Fr > 1$. This means that disturbances generated downstream of the

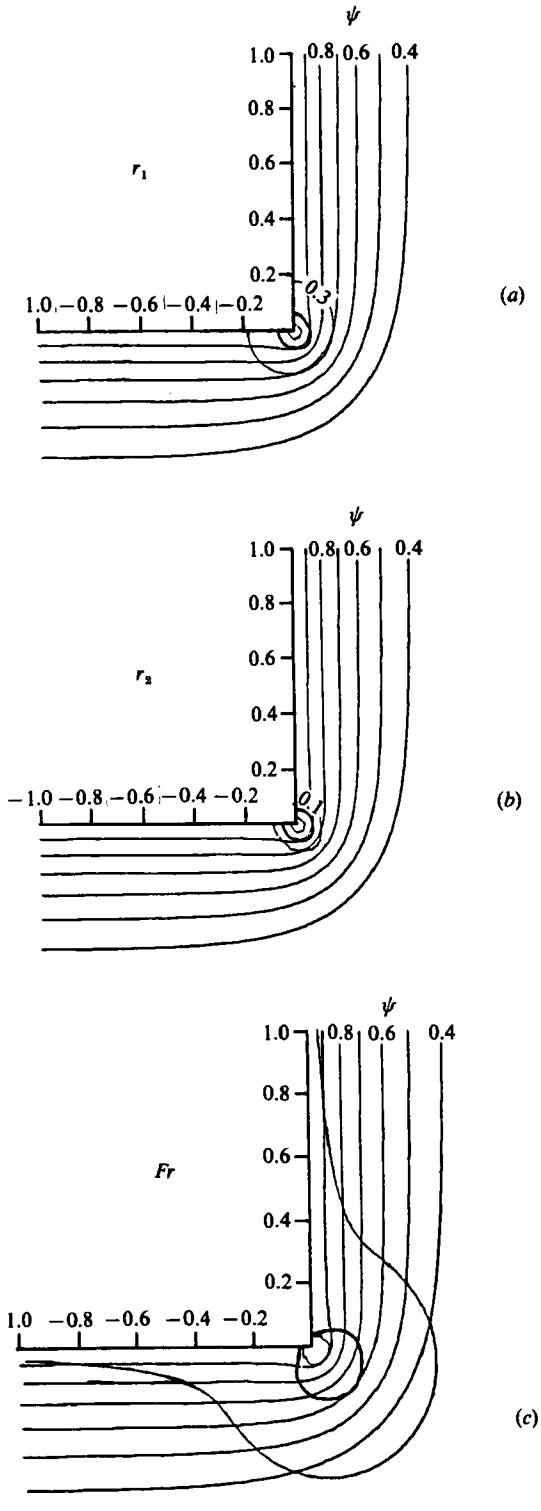

FIGURE 9. Contours of (*a*) $r_1 = |h_1/h_0| = 0.3, 1.0, 2.0$; (*b*) $r_2 = |U_1/U_0| = 0.1, 1.0, 3.0$ and (*c*) Froude number $Fr = 0.7, 1.0, 2.0$ (the critical value 1.0 is in bold), each superimposed upon streamlines $\psi = 0.4$ to 1.0 ($\epsilon = 0.5$).

corner cannot propagate upstream, which may cause a hydraulic jump near the second (downstream) $Fr = 1$ line. In our case, the conditions downstream are determined by the upstream parameters since, in the absence of another boundary close by, the Kelvin wave can propagate only with the boundary on its right. Hence, for this steady model, no hydraulic jump is expected as the flow re-enters the subcritical regime.

It should be pointed out, however, that while no stationary jump is predicted at a corner, travelling disturbances in the form of shock waves or bores are quite likely. These may arise, for example, when there is a sudden change in upstream conditions (like an increase in transport), in which case a fully nonlinear shock wave will be generated. According to Nof (1984), this shock would then propagate downstream (along a straight vertical boundary) at a speed larger than that of a Kelvin wave associated with both the disturbed and the undisturbed flow. Because the shock is faster than the sum of the downstream (with respect to the shock) advection speed and the downstream Kelvin wave speed but slower than the corresponding sum upstream of the shock, no energy is lost from the shock (except for small frictional losses) and the shock retains its form (Nof 1984). It is not clear however how such shock is transformed when it rounds a sharp corner. As in the case of monochromatic Kelvin waves (Packham & Williams 1968; Buchwald 1968; Miles 1972), one may expect that a certain amount of diffracted energy loss (Poincaré waves) will occur in its higher (super-inertial) frequency components. Thus the shock wave downstream of the corner will be less energetic and, possibly, of a different shape than when it was upstream of the corner.

3.5. *Separation*

The power-series expansion (2.24) is not valid very close to the apex. We rewrite (2.21)–(2.23):

$$h+\tfrac{1}{2}\epsilon w^2 = s+\tfrac{1}{2}\epsilon s^2, \tag{3.20}$$

$$1-\epsilon\left(w_{\mathrm{n}}+\frac{w}{r}\right) = \frac{h}{s}+\epsilon h, \tag{3.21}$$

$$-wh = ss_{\mathrm{n}}, \tag{3.22}$$

where $w = (u^2+v^2)^{\frac{1}{2}}$ is the speed, r is the radius of curvature of a streamline and the subscript n denotes a normal derivative. We now consider a boundary streamline, $s = 1$, and assume r_{c} to be the radius of curvature that causes its separation. Upon separation $h = 0$, and from (3.20) the speed $w = (1+2/\epsilon)^{\frac{1}{2}}$ is constant. From (3.21) we get

$$\epsilon\left(w_{\mathrm{n}}+\frac{w}{r_{\mathrm{c}}}\right) = 1 \tag{3.23}$$

i.e. the relative and the planetary vorticities are equal. Differentiating (3.20) in the normal direction, and substituting into (3.23) yields the momentum equation

$$-h_{\mathrm{n}}+\frac{\epsilon w^2}{r_{\mathrm{c}}} = w, \tag{3.24}$$

which states that the balance between the pressure gradient and the centrifugal force is held by the Coriolis force. Equation (3.24) is satisfied for any, however small, r_{c} (with a correspondingly steeper interface slope h_{n}). Therefore, this simple model does not give us the critical separation curvature. Calculations, which were done for smaller scales (of the order of $\epsilon^2 X$) near the apex (Cherniawsky 1985), show that, for

example, for $a = \frac{2}{3}$ and $\epsilon = 0.5$, $r_c < 0.02$ and hence the centrifugal upwelling is not important if the (dimensional) radius of curvature of the rounded corner is larger than about $0.1X$.

In this respect, we would like to point out that the centrifugal upwelling at a sharp cape, and the resulting doughnut-like shape of the interface (figure 7*c*) are exactly analogous to (hypothetical, since no one has ever observed them) anomalous warm eddies with a cold core, which have surfaced, for example, as a possible solution in Flierl's (1979) analytical two-layer model of the structure of warm- and cold-core rings. The balance of forces is the same – geostrophy on the outside and a cylostrophic balance on the inside. Figure 13 in Flierl (1979) shows a straight-line relation between the strength of the ring, as it was defined by Flierl: $\epsilon_F = -(2\epsilon+\epsilon^2)^{\frac{1}{2}}$, and its inside radius r_0. Although this line stops short of the $r_0 = 0$ axis (presumably owing to the singularity of his governing equation), it does seem to indicate that for $\epsilon_F > \approx -1.5$ ($\epsilon < 0.8$) the inner (cold) core of the ring disappears. In that case, the smaller centrifugal force is no longer sufficient to hold the inner slope for the upwelling to take place, and the ring stops being anomalous. Despite the differences, Flierl's constant-potential-vorticity (and hence deeper upper layer; see §2) radially symmetrical model seems to indicate that the horizontal extent of a centrifugal upwelling around a sharp re-entrant corner should be rather small for ϵ-values that are consistent (e.g. $\epsilon < \frac{1}{2}$) with the expansion (2.21). This agrees well with our results, and in particular with figure 7(*c*).

Because of its limited extent, the centrifugal upwelling is not the most likely cause of separation of the boundary streamline. Other effects may be more important. For example, if there is an adverse pressure gradient which raises the depth of the upper layer to its maximum value, $1+\frac{1}{2}\epsilon$, then from (3.20) we get a stagnation point, where $w = 0$, and hence separation. This pressure gradient could be caused by changes in buoyancy, wind forcing, or barotropic effects (e.g. changes in bathymetry). In addition, enhanced Ekman pumping (due to higher velocities at the corner) may contribute to upwelling and hence to separation. Consequently, a three-dimensional frictional model may be required to answer this question about the separation at a sharp cape. Merkine & Solan (1979) have shown that in the case of a uniform stream (V_c = constant) of depth H past a circular cylinder of diameter D and for a small Rossby number, $Ro = V_c/fD \ll 1$ (i.e. large D, or small V_c), the flow separates at some point on the cylinder, $\theta < \pi$, if the ratio

$$(\tfrac{1}{2}E_v)^{\frac{1}{2}}/Ro = (\nu f)^{\frac{1}{2}}D/(2HV_c) < 1,$$

where E_v is the vertical Ekman number and ν is the eddy viscosity. For $\epsilon \approx \frac{1}{2}$, the condition $Ro \ll 1$ is equivalent to $X/D \ll 1$. Although this suggests that Merkine & Solan's (1979) results are not applicable to strong flows around sharp corners, an analogous approach may prove fruitful.

While the problem of separation remains to be solved, let us assume, for example, that the flow does separate. This results in an anticyclonic baroclinic jet that would impinge on the straight coastline (downstream of the corner) at some non-zero angle. But, since the speed on the free streamline ($s = 1$, $h = 0$ for the inviscid model) is finite, it cannot pass through a stagnation point and hence it must turn right, away from the boundary (figure 10*a*). A transient adjustment process follows, whereby part of the flow pours into a closed gyre, while a different streamline, $s < 1$, passes through a stagnation point. As the size and the depth of the gyre increase, higher-valued streamlines move through the stagnation point. An equilibrium is

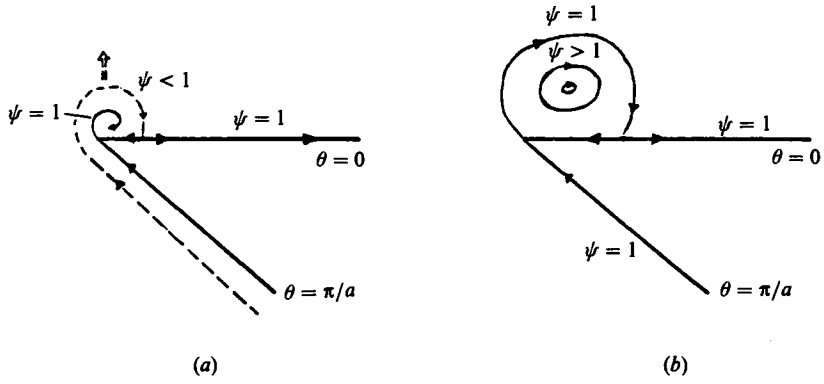

FIGURE 10. Conceptual drawing of the boundary streamline $\psi = 1$ (*a*) just after separation and (*b*) after its re-attachment.

reached, when the depth of the separated streamline attains its maximum value, $h = 1 + \frac{1}{2}\epsilon$, which allows it to pass through the stagnation point (figure 10*b*). In this context, the work of Whitehead (1985) on the deflection of a baroclinic jet by a wall becomes relevant. His results indicate that upon impingement the flow bifurcates, with a larger part turning to the right, in support of the above description of the adjustment process. The final size of the gyre may be a function of the wedge angle, the Rossby number, and the interfacial friction. Additional evidence for gyre formation behind a re-entrant corner was given by the experiments of Whitehead & Miller (1979) and of Kawasaki & Sugimoto (1984). Although friction and different upstream depth profiles do not allow for a detailed comparison between these experiments and our results, Kawasaki & Sugimoto's (1984) results indicate that the gyre is formed for Rossby numbers greater than 0.5 (with some dependence on the Ekman number), while for smaller Rossby numbers the coastal jet stays attached to the wall. We note that our qualitative description of the formation of the gyre is based on the assumption that the Bernoulli's function $G(\psi)$ and the potential vorticity function $K(\psi)$ remain invariant during the adjustment process, which may not be entirely true. If generation of some type of gravity waves accompanies the process, then the energy and the final size of the gyre will be affected. However, it is conceivable that for certain upstream conditions the free streamline could turn away from the boundary (i.e. to the left), forming a free jet, in which case there will be no re-attachment.

4. The case of more complicated geometries

The corner solution, given in the previous section, is readily extended to coastlines, which are composed of two or more corners, as long as no two corners are closer than about one (non-dimensional) unit. We invoke this restriction because of the nonlinear behaviour of the corner solution up to distances of $0.5X$ from the apex (figure 6*d*), and because, for $r < 1$, the normal derivative of the diffraction term $F(\theta)$ does not vanish at the boundary $\theta = 0$ (figure 4*a*). For the case of a channel mouth, this restriction of minimum width can be relaxed if the nonlinear terms are small ($\epsilon \ll 1$). We chose two examples to demonstrate the method.

4.1. *Circulation in the mouth of a channel*

LeBlond (1980) showed that in the case of a wide channel two baroclinic jets can coexist independently on opposite sides of the channel. In this respect, it may be convenient to classify channels into 3 categories: (i) narrow channels, narrower than the Rossby radius of deformation; (ii) intermediate channels, of widths between 1 and 3 Rossby radii; and (iii) wide channels, with widths larger than 3 Rossby radii. In the case when Rossby radii are different on opposite sides of the channel, some mean value can be used. In the absence of additional dynamical constraints (e.g. adverse pressure gradients), the last category of a wide channel is trivial, since the two jets do not interact at all. In order to give a simple example, we choose the case of a channel of intermediate width, whose sides are at a right angle to the coastline. We orient the axes so that the two sides are parallel to the negative x-axis, with the origin halfway between the two corners. Ignoring the $O(\epsilon)$ terms, the total solution $\psi = p^{\frac{4}{3}}$ is built as a linear superposition of two corner solutions,

$$p = B_1 p_1 + B_2 p_2. \tag{4.1}$$

Our solutions are not valid in small areas around each sharp re-entrant corner. We can overcome this problem by rounding these corners, so that the areas in question are removed from the domain of the solution. In order to round off the apex of each corner, p_1 and p_2 were rescaled by factors, which we call recession parameters, of $\exp(1.5\delta_1)$ and $\exp(1.5\delta_2)$ respectively. Each $\delta_i > 0$ $(i = 1, 2)$ is actually the distance between the side of the (recessed) corner and the boundary streamline $\psi = 1$ (away from the apex).

The constants B_1 and B_2 are calculated (for this case of a non-divergent channel) from the requirement that far inside the channel

$$p(x, d) = 1$$

and

$$p(x, -d) = 1 + B = (1 + A)^{\frac{3}{4}}, \tag{4.2a, b}$$

where $2d$ is the width of the channel, A (> 1) is the additional transport out of the channel and B is defined by (4.2b). For large negative x we have $p_1 = \exp[-1.5(-y + d + \delta_1)]$ and $p_2 = \exp[-1.5(y + d + \delta_2)]$. Assuming for simplicity that p_1 and p_2 have equal radii of deformation and that $\delta_1 = \delta_2 = \delta$, we get from the two-point matching (4.1) and (4.2),

$$B_1 = \exp(1.5\delta)\frac{e^{3d} - (1 + B)}{2\sinh(3d)}, \tag{4.3a}$$

and

$$B_2 = \exp(1.5\delta)\frac{(1 + B)e^{3d} - 1}{2\sinh(3d)}, \tag{4.3b}$$

so that far inside the channel, where p is independent of x,

$$p = \frac{(1 + \frac{1}{2}B)\cosh(1.5y)}{\cosh(1.5d)} - \frac{\frac{1}{2}B\sinh(1.5y)}{\sinh(1.5d)}. \tag{4.4}$$

Note that while this two-point matching procedure is not exact, it results in only minor distortions of boundary streamlines and is very simple to implement. (Only if $d \approx 0.5$ and if $A \gg 1$, or $1 + A \ll 1$, the distortion may become large, in which case it is advisable to use different recession parameters, a larger one for a corner with a smaller transport.) Note that (4.4) is essentially Gill's (1977) equation (5.2), and is applicable to a channel of slowly varying cross-section.

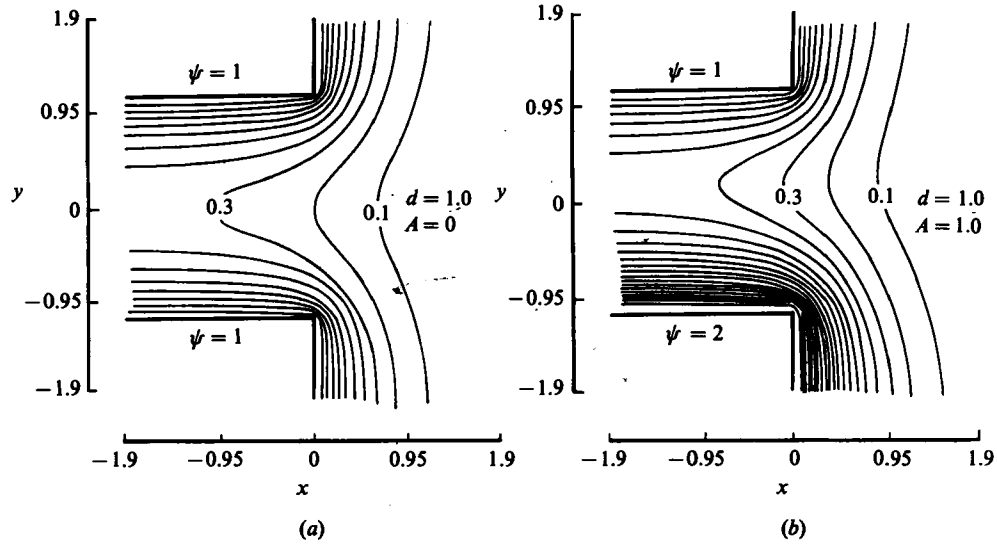

FIGURE 11. Circulation in the mouth of a channel: contours of the transport streamfunction ψ_0 for $d = 1.0$, $\delta = 0.1$: (*a*) $A = 0$, (*b*) $A = 1$.

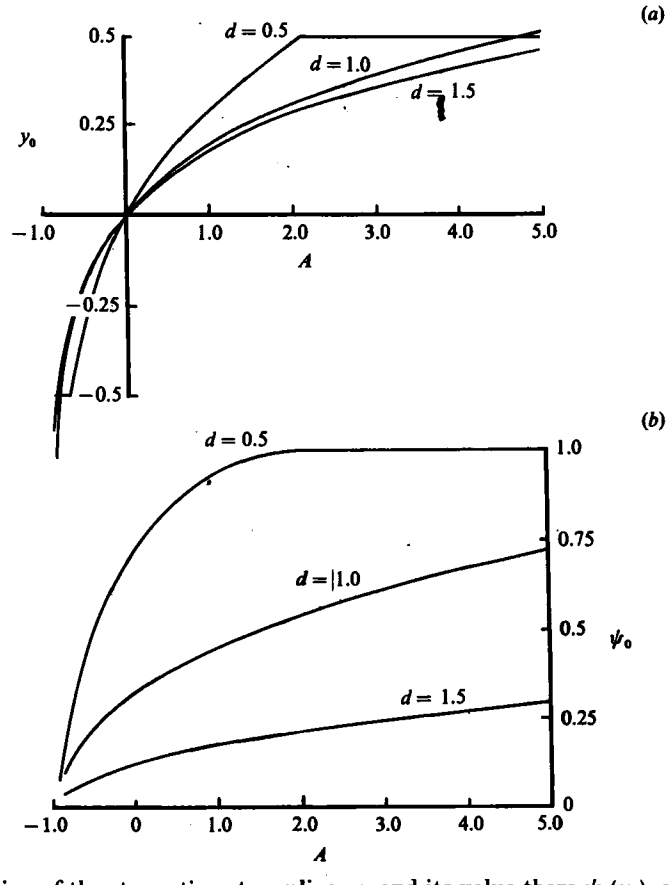

FIGURE 12. Location of the stagnation streamline, y_0 and its value there $\psi_0(y_0)$, as functions of the transport parameter A, for three values of channel width: $2d = 1$; $2d = 2$; and $2d = 3$.

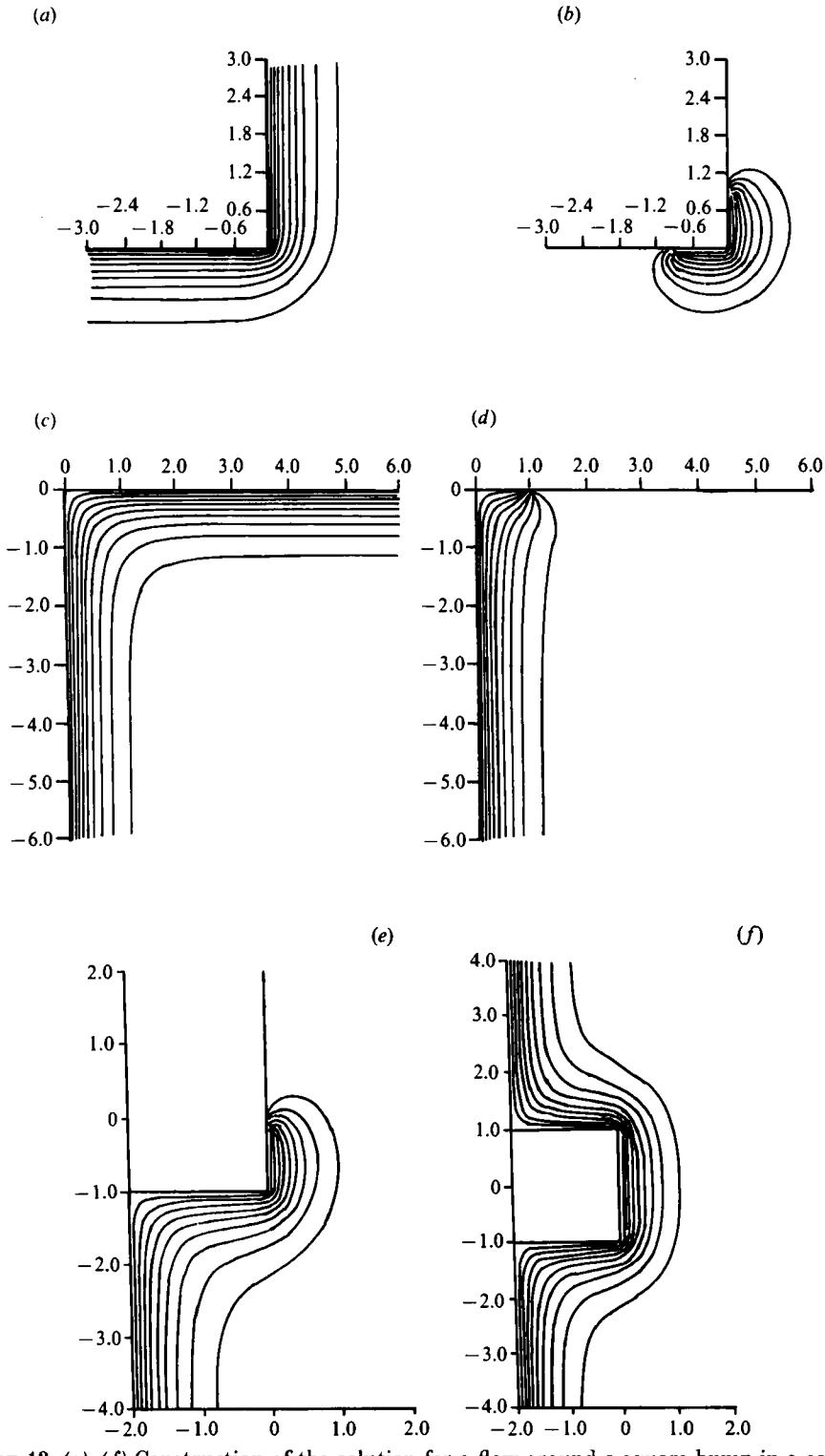

FIGURE 13. (a)–(f) Construction of the solution for a flow around a square bump in a coastline. The solution for a square bump in a channel is shown for (g) $A = 0$ and (h) $A = 1$.

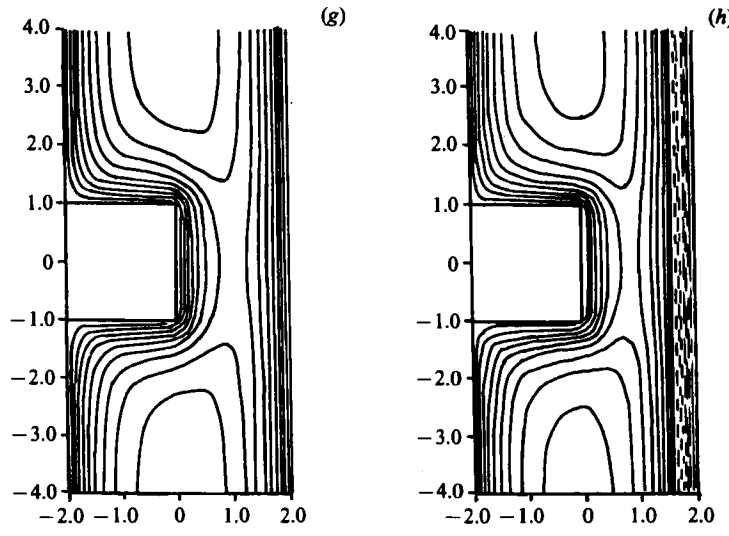

FIGURE 13(*g*) and (*h*). For caption see facing page.

Figures 11(*a*, *b*) show the resulting circulation for the case $d = 1$, $\delta = 0.1$, and for $A = 0$ (zero net outflow) and $A = 1$ (net outflow equal to the upstream transport). Only about 30% in the first case ($A = 0$) and about 40% in the second case ($A = 1$) of the upstream transport is recirculated across the mouth and out of the channel. The rest of the incoming transport continues up the channel. This is of course due to the dynamical control placed by the Rossby radius and the width of the channel upon the relative transports on the opposite sides. Differentiating (4.4), we find that p has a minimum at y_0, given by

$$\tanh(1.5y_0) = \frac{B}{(2+B)} \operatorname{cotanh}(1.5d). \tag{4.5}$$

In that case $\psi(y_0)$ is, in effect, the fraction of the incoming transport that is deflected across and out of the channel. In particular, when $B = 0$ ($A = 0$), $y_0 = 0$ and $\psi(y_0) = [\operatorname{sech}(1.5d)]^{\frac{1}{2}}$. If $1 + B > \cosh(3d)$, then $y_0 > d$, and the flow is out of the channel even on the left bank (looking downstream). Similarly, when $0 < 1 + B < \operatorname{sech}(3d)$, then $y_0 < -d$, and the flow is uniformly into the channel. Figure 12(*a*) shows the relation between A and y_0 for three values of d: 0.5, 1.0 and 1.5 (which span the intermediate width category), while figure 12(*b*) displays corresponding values of $\psi(y_0) = p(y_0)^{\frac{1}{2}}$, the fraction of the incoming transport that is recirculated out of the channel.

Similarly, in the case of a channel with diverging coastlines, the same two-point matching technique can be applied to the corners themselves, in which case $2d$ is the distance between the two apices.

4.2. *Flow around a square bump*

In order to construct a solution for the second example, we start with two corner solutions: one for the $\frac{3}{2}\pi$ ($a = \frac{2}{3}$) re-entrant corner, which was described in detail in §3, and the other for an inside $\frac{1}{2}\pi$ ($a = 2$) corner. In addition, we use source and sink

transport stream functions, $2F(\theta)$ and $2F(\pi-\theta)$, for a straight ($a = 1$) coastline. The procedure is best described graphically, as shown in figures 13(*a–f*). We first subtract the source and sink functions, $2F(\theta)$ and $2F(\pi-\theta)$, from the re-entrant corner solution (figure 13*a*), one unit distance upstream and downstream of the apex. This gives us the source and sink flow, shown on figure 13(*b*). Deleting the sink function $2F(\pi-\theta)$ from the inside-corner solution (figure 13*c*), one unit distance upstream of the apex, yields the source flow, shown on figure 13(*d*). Combining the last source with the sink on figure 13(*b*) gives us the source flow, which is shown on figure 13(*e*). Finally, combining this source with its image (in the x-axis) sink and raising to the power $\frac{4}{2}$ results in ψ, the flow about the 2×2 square bump, as shown on figure 13(*f*). However, subtracting a source and a sink at a point on a straight boundary is equivalent to subtracting an exponential profile from that boundary. In other words, instead of using sources and sinks in the above procedure, one can simply add two corner solutions with a common boundary, and then subtract the resulting surplus exponential current profile from that boundary. The restriction of the common boundary being at least one unit long stands as before, since the procedure is no longer valid close to the corners, where the profile is not exponential.

It is trivial to add a current in the opposite direction, which is (say) bounded by a wall 2 units away from the bump. The resulting baroclinic circulation around a square bump in a wide channel is shown on figures 13(*g*) (the case of equal transports) and 13(*h*) (double transport in the opposite direction). Note that about 30% of the incoming transport in the first case, and about 40% in the second case, is diverted back upstream by the opposing current. This is the same recirculation as in the case of the channel mouth (figures 11*a*, *b*) and is caused by the dynamical constraint due to the scale of the Rossby radius of the flow.

5. Discussion

From the nonlinear conservation equations that govern an inviscid upper-layer flow in a two-layer rotating fluid, we obtained the first two terms of the perturbation expansion which represents the solution to the problem of a flow around an arbitrary corner. It was found that the $O(1)$ term is geostrophic and, except for narrowing (widening) of the flow near a re-entrant (inside) corner, it does not differ qualitatively from the flow upstream. The effects of the nonlinear (advection) terms in the equation of motion become quite evident when the $O(\epsilon)$ term is added to the $O(1)$ term: the flow widens (for re-entrant corners) owing to the centrifugal acceleration of the fluid and, in addition, the depth of the upper layer decreases to almost zero near the apex of the corner (although we did not calculate this explicitly, we assume that near inside corners the effect is opposite: the $O(\epsilon)$ terms cause some increase in the depth). This is a manifestation of the centrifugal upwelling (downwelling). This upwelling is only important for relatively sharp corners. The validity of the solution and the continuity of the boundary streamline (i.e. the absence of separation) require that the sharp apex of the re-entrant corner be blunted to a certain extent. This can be successfully accomplished if one of the neighbouring streamlines is assumed to be the physical boundary, the choice depending upon the required radius of curvature. Using these recessed corner solutions we were able to generate streamlines of plausible flows in more general domains: inside channel mouths and around coastal indentations.

Further improvements to the present model will come from the incorporation of alongshore pressure-gradients effects. These may be due to changes in buoyancy (e.g.

due to coastal sources), or due to compression of the vortex lines by changes in the total depth. For example, in the case of a 'long' bathymetry (horizontal scale L much larger than X), we may use a method similar to that of Cushman-Roisin & O'Brien (1983) and apply a perturbation expansion in a small parameter X/L. For $X/L \ll \epsilon < 1$, the full corner solution is still valid locally near each corner, including the $O(\epsilon)$ terms, except that k (e.g. in (3.9)) is modulated (in the WKB sense) by changes in bathymetry, If $X/L \approx \epsilon$, then the $O(\epsilon)$ equation (3.10) must also be modified to include these barotropic effects.

Effects stemming from the variability of the flow were not included in the present study. For example, the criterion for separation of the flow at a sharp cape would have to be modified if the sum of residual and tidal currents were sufficient to cause separation at some stage of the tide. Once separated, the flow is likely to remain that way, even during reversals of the tide. This is due to the adverse pressure gradient from the closed gyre (see figure 10*b*) that is likely to appear on the downstream side of the cape. It is quite possible that this mechanism may be responsible for the separation of the Gibraltar surface flow from the right bank as it enters the Alborán Sea. A detailed investigation of the available data and models of rotating flows around re-entrant corners with variable depth may provide an answer to this question.

This work was funded by the Natural Sciences and Engineering Research Council of Canada under Strategic Grant G-0750.

Appendix. Derivation of the $O(\epsilon)$ equation for s_1

We derive an equation for s_1, treating s_0 as a known function of x and y. If we add (2.25*c*) to (2.26*c*) and use (2.28)–(2.30), we get

$$(s_0 v_1)_x - (s_0 u_1)_y + s_1 \nabla^2 s_0 = 2 s_0 s_1 + s_0 h_1. \tag{A 1}$$

But, from (2.27*b*),

$$(s_0 v_1)_x - (s_0 u_1)_y = \nabla^2(s_0 s_1) - h_1 \nabla^2 s_0 - \nabla s_0 \cdot \nabla h_1, \tag{A 2}$$

so that

$$\nabla^2(s_0 s_1) - h_1 \nabla^2 s_0 - \nabla s_0 \cdot \nabla h_1 + s_1 \nabla^2 s_0 = 2 s_0 s_1 + s_0 h_1. \tag{A 3}$$

We eliminate h_1 in favour of s_1 using (2.32), which also gives

$$\nabla s_0 \cdot \nabla h_1 = \nabla s_0 \cdot \nabla s_1 + s_0 (\nabla s_0)^2 - \tfrac{1}{2} (\nabla s_0 \cdot \nabla) (\nabla s_0)^2, \tag{A 4}$$

from which (2.35), the equation for s_1, follows:

$$s_0 \nabla^2 s_1 + \nabla s_0 \cdot \nabla s_1 + (\nabla^2 s_0 - 3 s_0) s_1 = W,$$

where

$$W = \tfrac{1}{2} (\nabla^2 s_0 + s_0) [s_0^2 - (\nabla s_0)^2] + s_0 (\nabla s_0)^2 - \tfrac{1}{2} (\nabla s_0 \cdot \nabla) (\nabla s_0)^2. \tag{A 5}$$

But, from (2.31)

$$\nabla^2 s_0 + s_0 = \frac{s_0^2 - (\nabla s_0)^2}{2 s_0}, \tag{A 6}$$

so that W simplifies to (2.36)

$$W = \frac{[s_0^2 - (\nabla s_0)^2]^2}{4 s_0} + s_0^3 - \tfrac{1}{2} (\nabla s_0 \cdot \nabla) (\nabla s_0)^2.$$

REFERENCES

BROMWICH, T. J. 1915 Diffraction of waves by a wedge. *Proc. Lond. Math. Soc.* **14**, 450–463.

BUCHWALD, V. T. 1968 The diffraction of Kelvin waves at a corner. *J. Fluid Mech.* **31**, 193–205.

CARRIER, G. F., KROOK, M. & PEARSON, C. E. 1966 *Functions of a Complex Variable: Theory and Technique*. McGraw-Hill.

CARSLAW, H. S. 1919 Diffraction of waves by a wedge of any angle. *Proc. Lond. Math. Soc.* **18**, 291–306.

CHARNEY, J. G. 1955 The Gulf Stream as an inertial boundary layer. *Proc. Nat. Acad. Sci.* **41**, 731–740.

CHERNIAWSKY, J. 1985 Rotating flows around sharp corners and in channel mouths. Ph.D. dissertation, University of British Columbia, Vancouver, B.C.

CUSHMAN-ROISIN, B. & O'BRIEN, J. J. 1983 The influence of bottom topography on baroclinic transports. *J. Phys. Oceanogr.* **13**, 1600–1611.

DRINKWATER, K. F. 1985 On the mean and tidal currents in Hudson Strait. *Atmosphere–Ocean* (in press).

FISSEL, D. B., LEMON, D. D. & BIRCH, J. R. 1982 Major features of the summer near-surface circulation of western Baffin Bay, 1978 and 1979. *Arctic* **35**, 189–200.

FLIERL, G. R. 1979 A simple model for the structure of warm and cold core rings. *J. Geophys. Res.* **84**, 781–785.

GILL, A. E. 1977 The hydraulics of rotating-channel flow. *J. Fluid Mech.* **80**, 641–671.

GILL, A. E. & SCHUMANN, E. H. 1979 Topographically induced changes in the structure of an inertial coastal coastal jet: application to the Agulhas Current. *J. Phys. Oceanogr.* **9**, 975–991.

GUTMAN, L. N. 1972 *Introduction to the Nonlinear Theory of Mesoscale Meteorological Processes* (translated from the Russian 1969 edn.). Israel Program for Scientific Translations, Jerusalem.

HUGHES, R. L. 1981 A solution technique for deep baroclinic rotating flows. *Dyn. Atmos. Oceans* **5**, 159–173.

HUGHES, R. L. 1982 On a front between two rotating flows which application to the Flores Sea. *Dyn. Atmos. Oceans* **6**, 153–176.

JANOWITZ, G. S. & PIETRAFESA, L. J. 1982 The effects of alongshore variation in bottom topography on a boundary current – (topographically induced upwelling). *Cont. Shelf Res.* **1**, 123–141.

KAWASAKI, Y. & SUGIMOTO, T. 1984 Experimental studies on the formation and degeneration processes of the Tsugaru Warm Gyre. In *Ocean Hydrodynamics of the Japan and East China Seas* (ed. T. Ichiye). Elsevier Ocenogr. Ser. No. 39, pp. 225–238. Elsevier.

LEBLOND, P. H. 1980 On the surface circulation in some channels of the Canadian Arctic archipelago. *Arctic* **33**, 189–197.

LEBLOND, P. H., OSBORN, T. R., HODGINS, D. O., GOODMAN, R. & METGE, M. 1981 Surface circulation in the western Labrador Sea. *Deep-Sea Res.* **28 A**, 683–693.

MACDONALD, H.M. 1915 A class of diffraction problems. *Proc. Lond. Math. Soc.* **14**, 410–427.

MARKO, J. R., BIRCH, J. R. & WILSON, M. A. 1982 A study of long-term satellite-tracked iceberg drifts in Baffin Bay and Davis Strait. *Arctic* **33**, 234–240.

MERKINE, L.-O. & SOLAN, A. 1979 The separation of flow past a cylinder in a rotating system. *J. Fluid Mech.* **92**, 381–392.

MILES, J. W. 1972 Kelvin waves on oceanic boundaries. *J. Fluid Mech.* **55**, 113–127.

NOF, D. 1978*a* On geostrophic adjustment in sea straits and wide estuaries: theory and laboratory experiments. Part I: One-layer system. *J. Phys. Oceanogr.* **8**, 690–702.

NOF, D. 1978*b* On geostrophic adjustment in sea straits and wide estuaries: theory and laboratory experiments. Part II: Two-layer system. *J. Phys. Oceanogr.* **8**, 861–872.

NOF, D. 1984 Shock waves in currents and outflows. *J. Phys. Oceanogr.* **14**, 1683–1702.

NOF, D. & OLSON, D. B. 1983 On the flow through broad gaps with application to the Windward Passage. *J. Phys. Oceanogr.* **30**, 1940–1956.

OBERHETTINGER, F. 1954 Diffraction of waves by a wedge. *Commun. Pure Appl. Math.* **7**, 551–563.

PACKHAM, B. A. & WILLIAMS, W. E. 1968 Diffraction of Kelvin waves at a sharp bend. *J. Fluid Mech.* **34**, 517–530.

PEDLOSKY, J. 1979 *Geophysical Fluid Dynamics*. Springer.

ROED, L. P. 1980 Curvature effects on hydraulically driven inertial boundary currents. *J. Fluid Mech.* **96**, 395–412.

ROSEAU, M. 1967 Diffraction by a wedge in an anisotropic medium. *Arch. Rat. Mech. Anal.* **26**, 188–218.

SANDERSON, B. G. & LEBLOND, P. H. 1984 The cross-channel flow at the entrance of Lancaster Sound. *Atmosphere-Ocean* **22**, 484–497.

SOMMERFELD, A. 1896 Mathematische theorie der diffraction. *Math. Ann.* **47**, 317–341.

SOMMERFELD, A. 1954 *Optics*. Academic.

STAKGOLD, I. 1968 *Boundary Value Problems of Mathematical Physics*, vols I and II. Macmillan.

STOMMEL, H. 1965 *The Gulf Stream*, 2nd edn. University of California Press.

STOMMEL, H. & LUYTEN, J. 1984 The density jump across Little Bahama Bank. *J. Geophys. Res.* **89**, 2097–2100.

WHIPPLE, F. J. W. 1916 Diffraction by a wedge and kindred problems. *Proc. Lond. Math. Soc.* **16**, 94–111.

WHITEHEAD, J. A. 1985 The deflection of a baroclinic jet by a wall in a rotating fluid. *J. Fluid Mech.* **157**, 79–93.

WHITEHEAD, J. A., LEETMAA, A. & KNOX, R. A. 1974 Rotating hydraulics of strait and sill flows. *Geophys. Fluid Dyn.* **6**, 101–125.

WHITEHEAD, J. A. & MILLER, A. R. 1979 Laboratory simulation of the gyre in the Alborán Sea. *J. Geophys. Res.* **84**, 3733–3742.